



HAL
open science

A Hydrogel/Carbon-Nanotube Needle-Free Device for Electrostimulated Skin Drug Delivery

Jean-François Guillet, Emmanuel Flahaut, Muriel Golzio

► **To cite this version:**

Jean-François Guillet, Emmanuel Flahaut, Muriel Golzio. A Hydrogel/Carbon-Nanotube Needle-Free Device for Electrostimulated Skin Drug Delivery. *ChemPhysChem*, 2017, 18 (19), pp.2715-2723. 10.1002/cphc.201700517. hal-01963158

HAL Id: hal-01963158

<https://hal.science/hal-01963158v1>

Submitted on 21 Dec 2018

HAL is a multi-disciplinary open access archive for the deposit and dissemination of scientific research documents, whether they are published or not. The documents may come from teaching and research institutions in France or abroad, or from public or private research centers.

L'archive ouverte pluridisciplinaire **HAL**, est destinée au dépôt et à la diffusion de documents scientifiques de niveau recherche, publiés ou non, émanant des établissements d'enseignement et de recherche français ou étrangers, des laboratoires publics ou privés.



Open Archive Toulouse Archive Ouverte (OATAO)

OATAO is an open access repository that collects the work of Toulouse researchers and makes it freely available over the web where possible

This is an author's version published in: <http://oatao.univ-toulouse.fr/21001>

Official URL: <https://doi.org/10.1002/cphc.201700517>

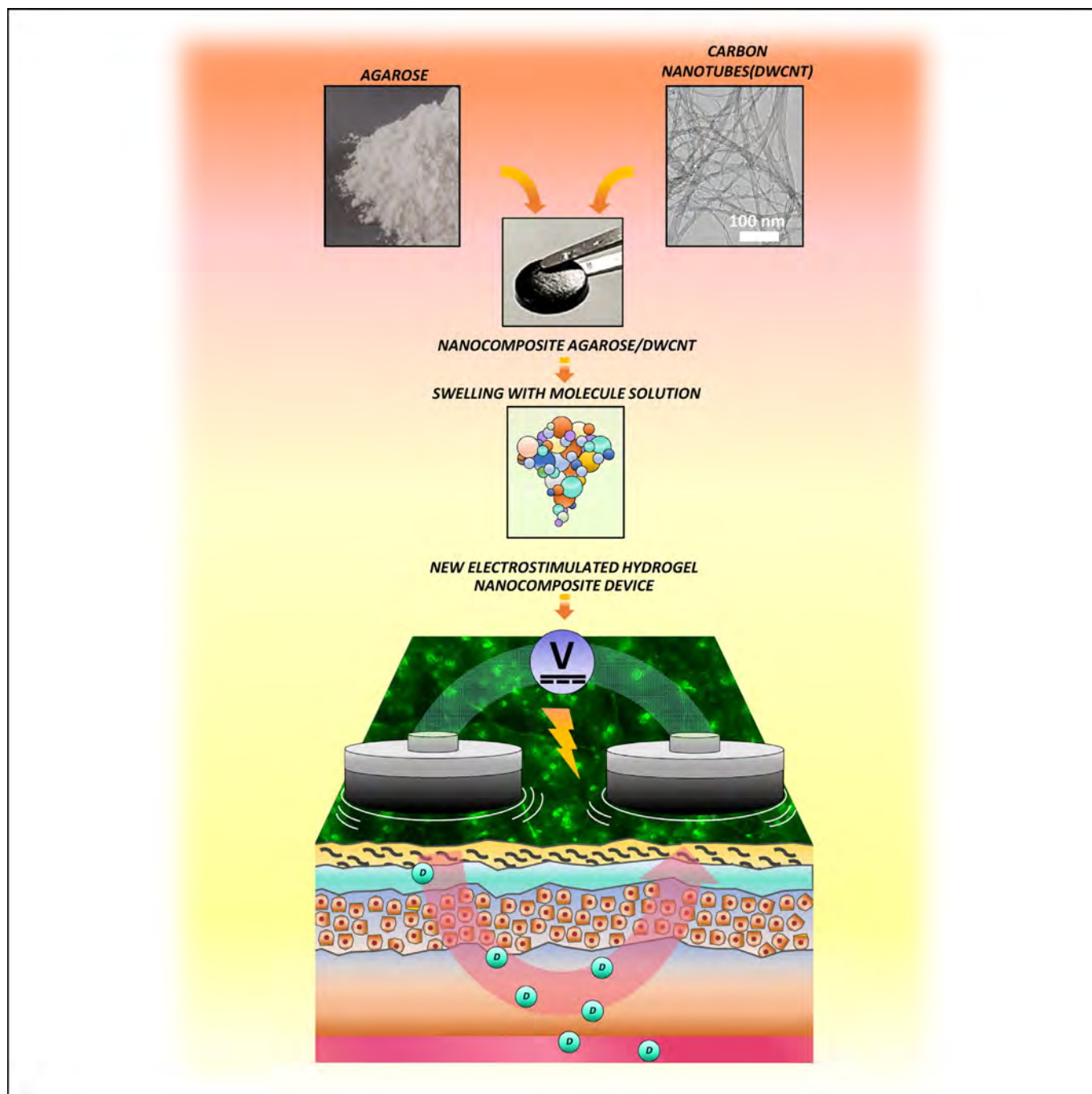
To cite this version:

Guillet, Jean-François[✉] and Flahaut, Emmanuel[✉] and Golzio, Muriel *A Hydrogel/Carbon-Nanotube Needle-Free Device for Electrostimulated Skin Drug Delivery*. (2017) *ChemPhysChem*, 18 (19). 2715-2723. ISSN 1439-4235

Any correspondence concerning this service should be sent to the repository administrator: tech-oatao@listes-diff.inp-toulouse.fr

A Hydrogel/Carbon-Nanotube Needle-Free Device for Electrostimulated Skin Drug Delivery

Jean-François Guillet,^[a, b] Emmanuel Flahaut,^{*[a]} and Muriel Golzio^{*[b]}



The permeability of skin allows passive diffusion across the epidermis to reach blood vessels but this is possible only for small molecules such as nicotine. In order to achieve transdermal delivery of large molecules such as insulin or plasmid DNA, permeability of the skin and mainly the permeability of the *stratum corneum* skin layer has to be increased. Moreover, alternative routes that avoid the use of needles will improve the quality of life of patients. A method known as electroporation has been shown to increase skin permeability. Herein, we report the fabrication of an innovative hydrogel made of a nanocomposite material. This nanocomposite

1. Introduction


The natural permeability of the skin allows selective passive diffusion across the epidermis to reach blood vessels. The characteristics of the skin (age, location and integrity) and of the penetrants (size, solubility and charge) affect the kinetics of percutaneous penetration.^[1] Small amphiphilic molecules such as nicotine (ca. 163 Da) are able to permeate through the skin thanks to their hydrophilic and hydrophobic parts. In order to achieve transdermal delivery of larger and more hydrophilic molecules such as insulin or plasmid DNA, permeability of the skin and mainly the permeability of *stratum corneum* has to be increased. Therefore, developing a transdermal drug delivery (TDD) system is a challenging task considering the selective permeability of the skin and the physicochemical properties of the drugs. Advancements in TDD systems are possible at different levels by judicious selection of drugs that can cross the skin at therapeutic rates without enhancement, by increasing skin permeability and driving forces for transdermal transport of small molecules or by enabling transdermal delivery of small and large hydrophilic drugs through targeted permeabilisation of the *stratum corneum* of the skin.^[2,3] In order to overcome the skin barrier, different drug delivery devices have been designed to deliver drug molecule by using physical methods such as electrical devices, optical devices, high-pressure devices, acoustic, thermal and microneedles devices.^[4–6] Some of them exhibit a significant increase in delivery of macromolecules across the skin. More precisely, a method named “electro-

device aims to permeabilise the skin and deliver drug molecules at the same time. It includes a biocompatible polymer matrix (hydrogel) and double-walled carbon nanotubes (DWCNTs) in order to bring electrical conductivity and improve mechanical properties. Carbon nanotubes and especially DWCNTs are ideal candidates, combining high electrical conductivity with a very high specific surface area together with a good biocompatibility when included into a material. The preparation and characterization of the nanocomposite hydrogel as well as first results of electrostimulated transdermal delivery using an ex vivo mouse skin model are presented.

permeabilisation” or “electroporation” has been shown to strongly increase skin permeability. This is a physical method where the application of electric pulses by means of electrodes is used to transiently increase the permeability of the cell membrane so that large molecules can enter into the cells.^[7] The method was developed in the 1980s^[8] and has since evolved to be used in the routine transfection of cells in vitro and different tissues, including tumours in vivo.^[9–13] During electroporation of the skin, the *stratum corneum* (SC) is modified leading to increases in electrophoretic mobility, molecular diffusivity, and electrical conductivity. It has been observed that high voltage pulsed electric fields can be more effective in enhancing transdermal flux of drugs in comparison with continuous application of low voltage pulses as in the case of iontophoresis.^[14] Electroporation-assisted transdermal transport depends on the shape, pulse repetition rate, amplitude, duration, number of electric pulses, electrode design, as well as the distance between electrodes.^[15–20] Earlier works proposed the creation of “pores” or aqueous pathways due to the electroporation procedure. The evolution of these pores was investigated by measurements of the electrical properties of the skin during pulse application.^[21,22] Short duration and high intensity pulses led to an alteration of the *stratum corneum* with nano- to micrometre-sized aqueous “pores”, whereas long duration and medium intensity pulses increased the permeability within the *stratum corneum* through large pores (up to hundreds of μm) but with lower density.^[23] The applied electric field provides an electrophoretic force for delivering molecules across the induced pores within the *stratum corneum*. Electrophoresis is the major component in the delivery of charged and large molecules across the skin.^[24,25] Electroporation mediated-TDD fully depends on the injection of the drug and on the type of electrodes used to enhance the permeability of the skin. To improve patient compliance, that is, avoid needle phobia, the application of a patch would be more likely accepted due to painlessness ability and as well for discretion. Other devices such as intradermal microneedle or multi-electrode arrays (MEA)^[26,27] have been designed to increase permeability of skin and reduce pain for patients.^[28] Effect of the electric field on drug diffusion was investigated to control drug delivery using different kinds of fluorescent molecules with various molecular weights, such as fluorescein isothiocyanate dextran (FITC).^[29] MEA devices showed an effective result on enhancement of plasmid expression for DNA vaccination.^[27] Nevertheless, alter-

[a] J.-F. Guillet, Dr. E. Flahaut
CIRIMAT
Université de Toulouse
CNRS, INPT, UPS, UMR CNRS-UPS-INP N° 5085
Université Toulouse 3 Paul Sabatier
Bât. CIRIMAT, 118 route de Narbonne, 31062 Toulouse cedex 9 (France)
E-mail: flahaut@chimie.ups-tlse.fr

[b] J.-F. Guillet, Dr. M. Golzio
Institut de Pharmacologie et de Biologie Structurale (IPBS)
UPS, CNRS, UMR 5089; BP 82164
205 route de Narbonne, 31077 Toulouse cedex 4 (France)
E-mail: Muriel.Golzio@ipbs.fr

 Supporting Information and the ORCID identification number(s) for the author(s) of this article can be found under:
<https://doi.org/10.1002/cphc.201700517>

An invited contribution to a Special Issue on Physical Chemistry in France

native devices avoiding the use of needles will improve the quality of life of patients during chronic administration and/or during vaccination. These devices should have two main properties: first having conductive properties in order to be used as electrodes and second being a reservoir for the drug to be delivered. Hydrogels are commonly used in drug delivery system thanks to their hydrophilic nature.^[30,31] They also own many useful properties such as swelling, great biocompatibility, low toxicity (if any) and possible biodegradability if desirable. Furthermore, these polymers may be cross-linked by different methods such as addition of poly electrolytes, pH variation, heating or by irradiation.^[32] In recent years, scientists have developed a wide range of innovative nanocomposite hydrogels by the addition of different nanoparticles such as gold, iron oxide, hydroxyapatite, and of course carbon nanomaterials including carbon nanotubes.^[33,34]

Carbon nanotubes (CNTs) are an allotrope of carbon in the form of cylindrical all-carbon molecules.^[35] CNTs, and especially double-walled-carbon-nanotubes (DWCNTs),^[36] are ideal candidates for many applications, combining high electrical conductivity with a very high specific surface area (ca. $1000 \text{ m}^2 \text{ g}^{-1}$) together with a good biocompatibility when included into a material, or deposited on a surface.^[37] They can be incorporated into different polymers in order to prepare nanocomposite materials. Actually, only a few papers report the use of CNTs in various experimental configurations for electro-stimulated drug delivery. For example, an *in vitro* study evaluated the transdermal delivery of clonidine (ca. 230 Da) mediated by a CNT-epoxy nanocomposite membrane by applying various electrical biases.^[38] Servant et al. reported the fabrication of two different carbon-based hydrogel nanocomposites with graphene based^[39] or multi-walled CNTs^[40] for *in vivo* pulsatile (low voltage) drug delivery systems (DDS). These devices were subcutaneously implanted and stimulated with electric field. Although these strategies are rather different from our work, they demonstrate the feasibility and high potential of application of CNTs (and nanocarbons in general) for electrostimulated drug delivery.

Here, we report the fabrication of an innovative needle-free device, made of DWCNTs-containing nanocomposite material. This nanocomposite device aims at permeabilising skin and delivering drug molecules simultaneously. It includes a biocompatible polymer matrix (hydrogel of agarose) and DWCNTs in order to improve both mechanical and electrical properties. The aim of this study was to prepare a DWCNT bio-based nanocomposite hydrogel, and its characterization in terms of structural organization, storage capacity and electrical properties. Finally, we show its first use as a TDD system after electro-stimulation using an *ex vivo* mouse skin model and a 4 kDa fluorescent FITC-dextran used as a control molecule. These encouraging results provide good evidence that the use of DWCNTs improves the transdermal delivery potentialities of the biocompatible polymer matrix.

2. Results and Discussion

2.1. Device Characterization

We first performed visual observations of CTRL-AG (Agarose) and DWCNT-AG (DWCNT-Agarose) hydrogel materials. Hydrogels were prepared using deionized (DI) water with 2.5 wt./v of agarose with 0, 0.1, 0.5, 1 wt.% of DWCNTs (DWCNT-AG hydrogels). After gelation, samples were deposited on a dry absorbing paper for macroscopic observation. As the concentration of DWCNTs increased, transparency of the hydrogel decreased and they became darker (Figure 1 a). After the drying step and the swelling step (Figure 1 b), the weight, thickness and diameter of DWCNT hydrogels were measured (Figure 2).

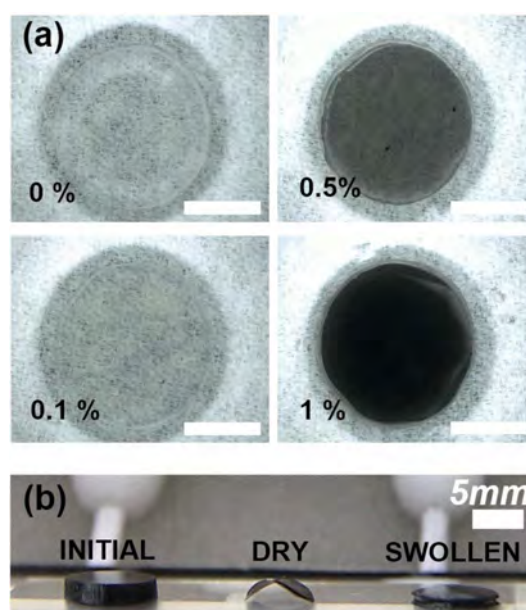


Figure 1. Visual characterization of hydrogel nanocomposite device. a) Macroscopic visualization of CTRL-AG hydrogel (agarose alone, 0% CNTs), 0.1 wt.%, 0.5 wt.% and 1 wt.% of DWCNTs in AG hydrogel nanocomposite. Scale bar = 5 mm. b) Picture of 1 wt.% DWCNT-AG hydrogel nanocomposite after manufacturing, drying and swelling in PBS.

2.2. Drying, Swelling and Morphological Characterization

Deformation of the material can occur during the drying step, and should be limited as much as possible. Many parameters such as temperature and hygrometry play a major role, as well as the nature of the interface with the substrate. After comparing different drying conditions (including the comparison between substrates of different nature such as glass, silicon wafer, Teflon, and various metals), we finally dried the hydrogels on a stainless steel substrate (INOX309) at 20–25 °C for 24 h at atmospheric pressure (Figure 1 b for DWCNT-AG, and Figure S1 for CTRL-AG). The weight, thickness and diameter of DWCNT hydrogels were measured (Figure 2a). We obtained similar results for CTRL-AG hydrogel and DWCNT-AG (1 wt.% DWCNT) hydrogel nanocomposite samples with 97% and 96.7% of water weight loss, resp. Thickness losses of 88.4%

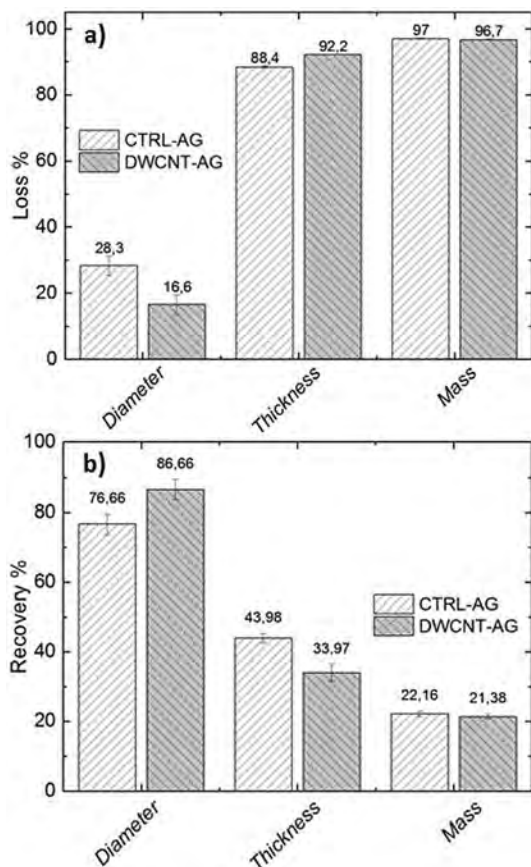


Figure 2. Characterization of the deformations of the CTRL-AG hydrogel and DWCNT-AG hydrogel nanocomposite (1 wt.% DWCNT) after drying and swelling (24 h in PBS) steps. a) Weight, thickness and diameter losses after the drying step for the CTRL-AG hydrogel and DWCNT-AG hydrogel nanocomposite [dry state/ initial state, calculated from Eq. (1)]; b) Weight, thickness and diameter recovery after the swelling step in PBS for the CTRL-AG hydrogel and DWCNT-AG hydrogel nanocomposites (swollen state/ initial state [calculated from Eq. (1)]).

and 92.2% were observed for CTRL-AG hydrogel and DWCNT-AG hydrogel nanocomposite, resp. Interestingly, the diameter decrease was only 16.6% in the presence of DWCNTs (28.3% in CTRL-AG), showing that the presence of DWCNTs in agarose absorbs deformation strains during the drying step. This mechanical strengthening thanks to the presence of DWCNTs mainly affects the diameter. This is important because this represents the surface which will be in contact with the skin during drug delivery.

Figure 2b shows recovery after 24 h of swelling step in phosphate buffer saline (PBS). Samples absorbed about the same amount of liquid (22% and 21% water weight for CTRL-AG and DWCNT-AG, resp.) Regarding the thickness, the gain was lower in the presence of DWCNTs (34% versus 44% for CTRL-AG) and the final diameter was also closer to that of the initial material in the presence of DWCNTs (86.6% versus 76.6% for CTRL-AG).

These results demonstrate that the presence of DWCNTs did not affect water weight recovery, and thus the capacity of the material to absorb and store a drug solution. Altogether, our

results show that our device can be used as a drug reservoir. Moreover, our method allows to limit diameter deformation and to maximize surface contact of the hydrogel with the skin and the electrode connections.

2.3. SEM Characterization

In order to assess the dispersion of DWCNTs in the polymer matrix (1 wt.% DWCNT-AG hydrogel), we performed FEG-SEM observation of the dry hydrogel nanocomposite. This revealed a high roughness topography at the surface of the sample, depicted in Figure 3a. DWCNTs were located under a thin layer of polymer (better evidenced in the inset in Figure 3a) attributed

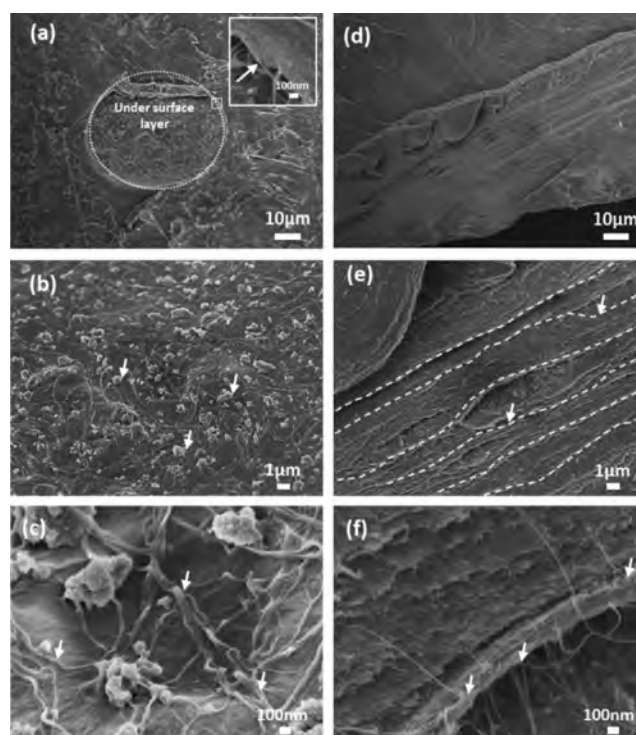


Figure 3. Microstructural characterization of hydrogel nanocomposites. SEM image of 1 wt.% DWCNT-AG hydrogel nanocomposite; a, b, c) Surface topography at X1000/X15000/X40000; c, d, e) Cross-sectional topography of hydrogel nanocomposite at X1000/X15000/X40000. Scale bars = 10 μm (a, d), 1 μm (b, e), 100 nm (c, f).

to a “skin effect” between polymer and DWCNTs, probably induced throughout the thermal gelation step of agarose. Actually, this very thin layer between surface and bulk material may correspond to an insulating part, expected to bring a potential capacitive barrier to our nanocomposite material. Figure 3b shows a magnification of the surface evidencing DWCNTs bundles, demonstrating clearly the efficient dispersion of the nanotubes. We also observed non-uniform agglomerates indicated by white arrows and corresponding to disorganized carbon, initially present in the DWCNT material. Figure 3c shows more details at higher magnification of the surface, where disorganized carbon (ca. 0.05–1 μm) and DWCNTs bundles indicated by white arrow (ca. 10–100 nm) are clearly visi-

ble. Figure 3d,e show a cross-section of the same sample evidencing a 3D hydrogel network formed by a superposition of agarose layers. Similarly, to what was evidenced at the surface, Figure 3f shows many DWNCTs bundles throughout the hydrogel nanocomposite, also evidencing a very efficient dispersion of the nanotubes across the matrix. These observations confirmed that the preparation process was reproducible and efficient, also suggesting that the DWCNT-AG hydrogel nanocomposite network was already interconnected at the gelling step suggesting that physical percolation in the dry state was reached. However, it is difficult to extrapolate the actual percolation conditions in the swollen state because the expansion of the material may lead to significant differences between the dry and wet states. It is also important to note that the incorporation of a large amount of water also modifies the actual CNT ratio within the material (significant decrease).

2.4. Swelling Behaviour

Because we hypothesize the possible use of this material for delivering different types of drugs or macromolecules, we investigated more in details its swelling behaviour in different media (deionised water, PBS) and at different pH values. The swelling ratio (g g^{-1}) in PBS was quantified as a function of time in Figure 4a. We observed for both samples a rapid swelling within the first 50 minutes to reach a plateau. The inset in Figure 4a shows a magnification of the swelling during the first hour and illustrates the influence of DWCNTs which slow-down the swelling for DWCNT-AG already after 10 min, probably because the presence of the nanotubes increases the stiffness of the polymer network. Swelling reached the maximum values of 6.4 g g^{-1} and 5.5 g g^{-1} , for CTRL-AG and DWCNT-AG hydrogels, respectively, after 24 h.

At the final swelling state (24 h), the hydrogel were considered as full, because samples could not expand substantially more. Only 1 g g^{-1} difference was observed between CTRL-AG and DWCNT-AG in terms of swelling. We suppose that swelling restriction was induced by the drying step and we suggest drying stress leading to an aggregation of the agarose chains throughout the matrix. Regarding the recovery ratio upon swelling, no variation was observed throughout the investigated pH range (Figure 4b). Sweeping pH value evidenced an operating window in terms of pH stability of our devices, which was expected for agarose. We recovered between 22.2% (CTRL-AG hydrogel) and 21.4% (DWCNT-AG) of the initial value in PBS.

2.5. Release Properties

As the device will be applied on the skin, we tested the hypothesis of a passive release from our samples. For that we used artificial sweat in order to mimic extreme physiological conditions. Samples were incubated in artificial sweat at 50°C to mimic a worst-case condition. The quantification of fluorescein isothiocyanate dextran (FITC-D) molecules release from the hydrogel was performed by fluorescence spectroscopy (Figure 5a). From weight measurements between the dry and

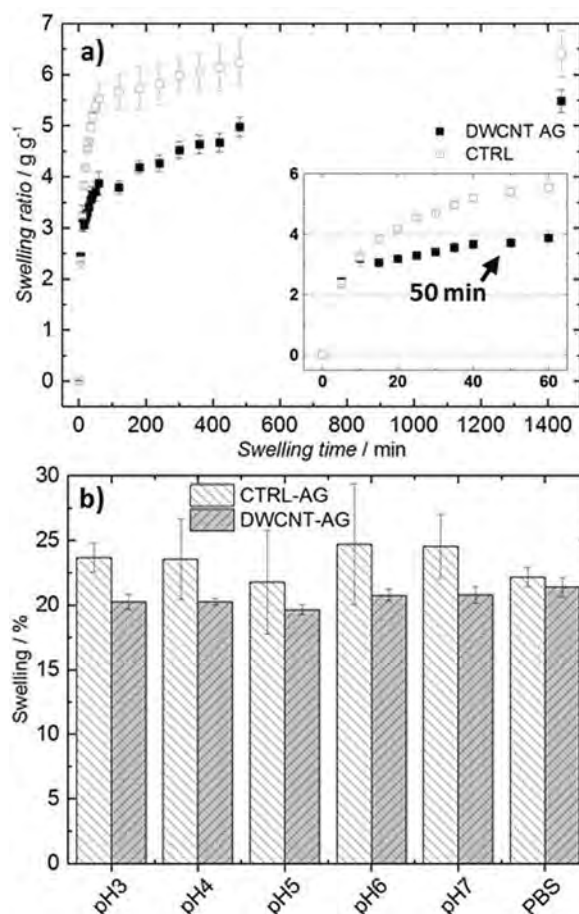


Figure 4. Swelling characterization for CTRL-AG hydrogel and DWCNT-AG hydrogel nanocomposite. a) Weight swelling ratio in PBS as function of time for CTRL-AG hydrogel and DWCNT-AG [1 wt.% DWCNTs, calculated from Eq. (1)]. b) Swelling recovery percentages as a function of different pH values ranging from 3 to 7 and in PBS solution (pH 7.4) at 24 h [swollen state/ initial state, calculated from Eq. (2)].

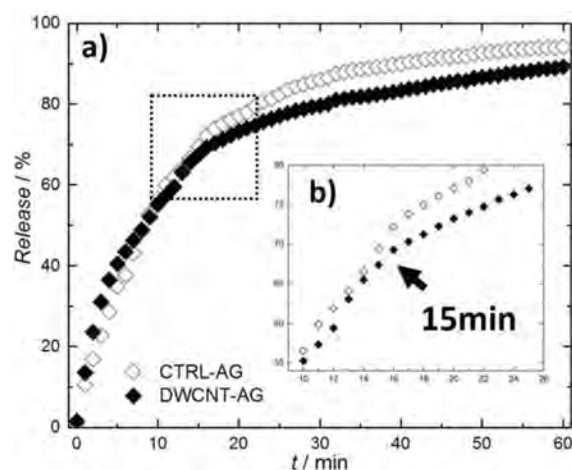


Figure 5. Release characterization of CTRL-AG hydrogel and DWCNT-AG hydrogel nanocomposite. a) Spectrophotometry measurement of the FITC-D release due to release % versus time from CTRL-AG hydrogel and DWCNT-AG hydrogel nanocomposites (1 wt.% DWCNTs) under stirring conditions over 60 min at 1 mM FITC-D concentration. b) Expanded portion showing the transitory area.

the swollen states, the amount of FITC-D (mol) initially loaded inside the hydrogel was calculated from an initial concentration of 1 mM FITC-D in PBS and reported in Table 1. We also calculated the amount released, and finally the release ratio.

Sample	FITC-D (swollen state) [mol]	FITC-D (released) [mol]	Release [%]
DWCNT-AG	2.93×10^{-8}	2.61×10^{-8}	89.2
CTRL-AG	2.83×10^{-8}	2.66×10^{-8}	94.2

Release versus time was plotted in Figure 5. The presence of DWCNTs did not significantly modify the release kinetics and in both cases, almost 70% of the FITC-D was passively released in about 15 min (Figure 5b), after what the phenomenon clearly slowed down with a slower release kinetics for the DWCNT-AG hydrogel (15 min). The maximum release reached ca. 94% within one hour. These results thus indicate that although the presence of DWCNTs influences the deformation upon drying, the nanotubes seem to play no obvious role in terms of passive release from the swollen material in these extreme conditions (100% artificial sweat and continuous stirring), very far from a realistic scenario.

2.6. Electrical Characterization

Electrical impedance spectroscopy (EIS) measurements revealed an ionic conductivity related to the presence of PBS solution inside the hydrogel materials (swollen), as shown in Figure 6. EIS measurement is an easy method to determine if DWCNT percolation threshold was reached. We measured a resistivity of 362 Ohm (2.7 ms cm^{-1}) for CTRL-AG hydrogel while the resistivity of the DWCNT-AG hydrogel nanocomposite was slightly lower at 307 Ohm (3.2 ms cm^{-1}). Although microscopy

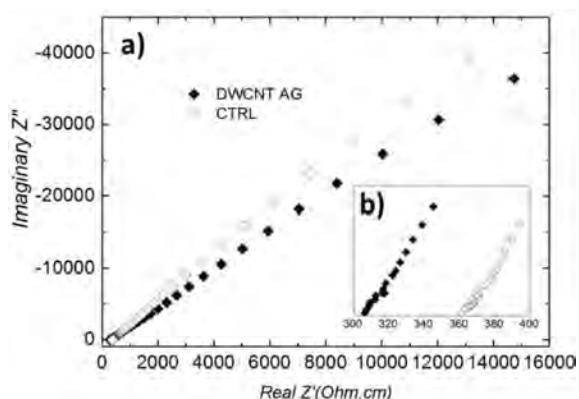


Figure 6. EIS characterization of the CTRL-AG and DWCNT-AG hydrogels (1 wt.% DWCNTs) in the swollen state. a) Measurement of ionic resistivity of CTRL-AG hydrogel and DWCNT-AG hydrogel nanocomposite. b) Expanded portion showing the low Z' range. Swollen hydrogels (24 h in PBS) were placed between two stainless steel electrodes and analysed in the range 1 Hz–1 MHz with an applied AC voltage of 100 mV at room temperature.

observations (Figure 3) revealed a good dispersion of DWCNT through the hydrogel nanocomposite, EIS measurement did not clearly evidence any percolation phenomena in the swollen state. Absence of a percolation threshold even at 1 wt.% loading of DWCNTs is surprising. Indeed, earlier work of our group involving the same DWCNTs but with a different matrix (Polyepoxy^[41]) revealed that the percolation threshold was reached at a much lower concentration (0.3 wt.%). However, the situation is indeed quite different here for many reasons: (1) the nanocomposite is not composed of only 2 phases (polymer matrix and CNT load), but 3 phases because the swollen nanocomposite is mainly composed of a third phase, which is water; (2) although the ratio of CNTs is 1 wt.% versus the polymer, the actual load in the swollen material is only 0.12 wt.% of the total mass ($\text{H}_2\text{O}/\text{polymer}$). EIS measurements performed in PBS before the drying step (Figure S2) evidenced the same behaviour, namely the absence of a percolation threshold. We observed an ionic dominant conduction behaviour for DWCNT-AG. Likewise, we observed a modest decrease in terms of ionic conductivity for DWCNT-AG, when we expected DWCNTs to create new and more efficient pathways through the hydrogel for ionic species, supposed to lead to an increase in ionic mobility. The electrical characterization measurement conditions are very far from the electroporation ones, indeed intensity of applied electric field could induce structural modification through the DWCNT-AG hydrogel nanocomposite network. The complexity of such a triphasic system (water/polymer/CNTs), especially in regard of electrical percolation of DWCNTs must be investigated by complementary techniques (currently in progress). EIS measurement method brings a first approach to understand the electrical behaviour of our nanocomposite hydrogel.

2.7. Skin Electroporation

Electro-stimulated release of FITC-D from 1 wt.% DWCNT-AG hydrogel nanocomposite and CTRL-AG hydrogel as a control were performed by electroporation on fresh mouse skin sample in order to break the highly resistive *stratum corneum* barrier layer.^[42] In the absence of an electric field (Figure 7a,d), very weak fluorescence was observed on the skin after 30 min of incubation suggesting that our device did not release much FITC-D without external stimulation. This means that when compared to the passive release observed in extreme conditions (total immersion in 100% artificial sweat and mechanical stirring), the 30 minutes' application on the skin did not lead to a drastic release of the FITC-D molecules. When electrical stimulation (10 pulses of 20 ms at 1 Hz frequency and 300 V) was applied an immediate contraction of mouse skin, corresponding to the electrical stimulation of the skin muscles located below the dermis skin layer, was observed. After 30 min, we observed as a result two fluorescent marks corresponding to the cathode (–) and the anode (+) positions (Figures 7b,e). Observation on the cathode electrode side revealed a strong fluorescent signal due to electrostimulation applied on the device, when in contrast only a weak fluorescence staining could be observed at the positive pole. Figure 7e clearly re-

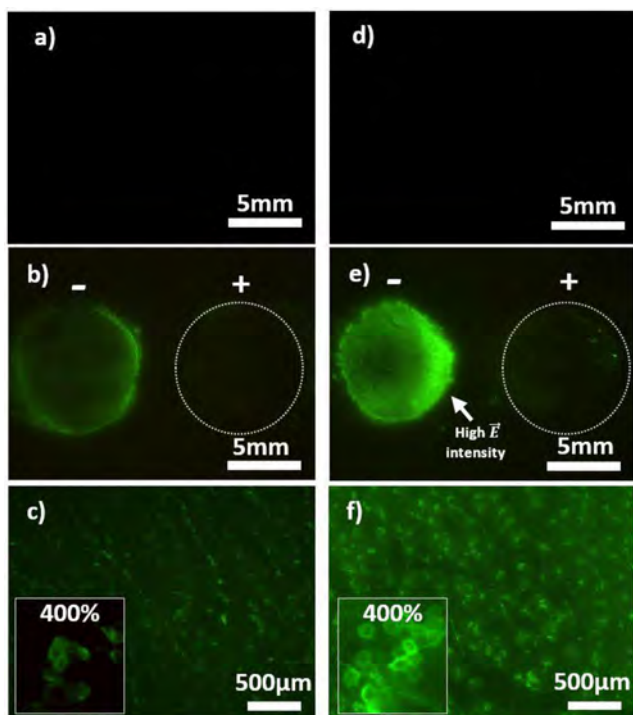


Figure 7. Visualization of skin electroporation. Representative pictures of mouse skin after electroporation with CTRL-AG and DWCNT-AG (1 wt.% DWCNTs) containing 4 kDa FITC-dextran at 1 mm. Images (a,d) show CTRL-AG and DWCNT-AG without electrical stimulation under identical conditions at the same intensity level (X0, 57). Images in (b,e) are with electrical stimulation: The anode is on the left-hand side and the cathode on the right-hand side (magnification X0.57). c, f) Magnifications (X4) of the anode area of (b, e), respectively. The frame on the left side of (c, f) pictures show a numerical magnification X400.

veals the electric field distribution in the case of the DWCNT-AG nanocomposite, with the expected presence of a fluorescent crescent on the electrodes' sides. These crescents reflect the electric field distribution intensities. Indeed, the electric field intensity is defined as the ratio between the applied voltage and the distance between the electrodes.^[8, 18, 28] Intensities were maximum between the two electrodes and decreased as the distance between the electrodes increased. Moreover, the circumference of electrodes exhibited higher fluorescence intensity. This increase may be due to the fact that the edges of the electrode were rough all-around the patch. In fact, we observe the formation of this roughness during the drying step. This may induce a "tip effect" on skin when electric field is applied. A stronger fluorescence staining was observed with the DWCNT-AG nanocomposite, unambiguously evidencing the role played by DWCNTs. We can thus expect a more effective destabilization of *stratum corneum* layer due to higher current density flow, combined with a more effective release of the FITC-D molecules. Visualization at higher magnification of the skin (Figure 7 f) revealed different structures such as hair follicles, marked wrinkles but also hexagonal nest-like shapes showing penetration through the *stratum corneum*. We can assume that the FITC-D molecule reached different *stratum corneum* layers according to the depth of penetration, but more intense or different kind of stimulations (such as iontophoresis

or electrophoresis) is probably required to reach the sublayer skin and finally the blood circulation. The visualization of these hexagonal nests and the heterogeneous FITC-D distribution indicate a dependence in terms of possible preferential pathways through the *stratum corneum* layer.

To our knowledge, these experiments are the first evidences of electroporation of mouse skin *stratum corneum* and release of FITC-D at the same time using such a device based on agarose polymer. The presence of 1 wt.% of DWCNTs inside the hydrogel is evidenced to significantly increase the penetration through the superficial layers of the skin.

However, there are earlier reports in the literature showing that the presence of carbon nanotubes allows decreasing the voltage threshold for electro-stimulated both in vitro and in vivo drug delivery.^[43,44] The authors describe the enhancement of the electric field (tip effect) by the carbon nanotubes as the main mechanism for the observed enhancement.

In our work, the carbon nanotubes are entrapped within the hydrogel, and we have demonstrated (not shown) that even in extreme conditions (artificial sweat at 50 °C), they are not released, so the mechanisms involved here are of a different nature.

Increasing the electrical conductivity of the material is probably the reason why the delivery is improved. Thorough investigation of skin structure after electrostimulation is in progress but still too preliminary to be included at this stage.

3. Conclusions

Addition of DWCNTs to an agarose hydrogel allows to prepare a nanocomposite material which can be at the same time used for storing a drug of interest and release it through the skin by electrostimulation (electroporation). The presence of the DWCNTs also improves the mechanical properties of the material, without however modifying too much its behaviour in terms of storage. Our process uses no solvent other than water, and the DWCNTs are very well dispersed within the agarose matrix. We have demonstrated the formulation of biocompatible electrodes for the transdermal delivery of large (4 kDa) molecules through the *stratum corneum* by electrostimulation. Although our investigations are currently limited to ex vivo data using a mouse skin model, we are convinced that this new material and these preliminary results are very promising for applications in the field of transdermal drug delivery. Work is in progress to optimize the electrostimulation conditions, as the idea of the inclusion of carbon nanotubes is also to be able to perform the delivery in much milder conditions, more compatible with a realistic clinical use.

Experimental Section

Device Fabrication

Agarose (AG) was purchased from Sigma-Aldrich. Hydrogel was prepared using deionised (DI) water so that the final concentration of AG was 2.5 wt./v. %. After solubilisation of AG, the solution was blended with DWCNTs at 0.1, 0.5, 1 wt.% of the polymer and processed using a shear-mixer (IKA, Ultra-Turrax T10, 20 min, 80 °C).

DWCNTs were prepared according to Flahaut et al. 2003. The suspensions were then poured into a Petri dish and cooled down to ambient conditions (20–25 °C) for 30 minutes. After cooling, hydrogel nanocomposites were shaped into cylinders of 1 cm diameter and 0.2 cm thickness, and placed into DI water (pH 5.5) bath in the fridge for preservation. The overall elaboration process is shown on Figure 8.

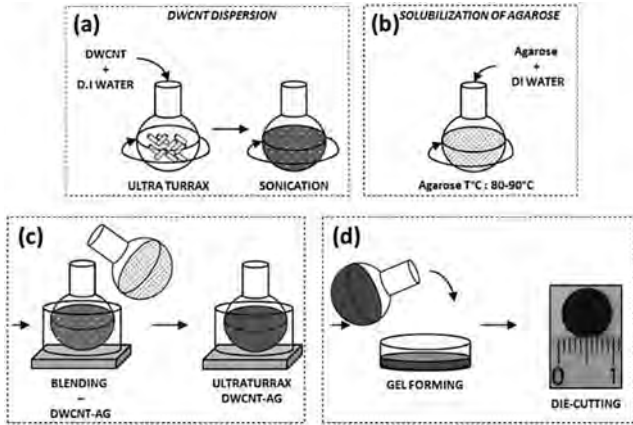


Figure 8. Schematic representation of DWCNT-AG nanocomposite hydrogel synthesis. a) Ultra-turrax dispersion of DWCNTs powder in 50 mL DI water for 20 min followed by sonication for 1 h at room temperature. b) Solubilisation of agarose powder in 50 ml of DI water at 90–100 °C. c) Agarose/DWCNTs blending directly followed by ultra-turrax homogenization for 20 min at 90–100 °C. d) Formation of the hydrogel nanocomposite by gelation at room temperature followed by die-cutting.

Characterization of the Device

Drying Method and SEM Preparation

Cylindrical samples were placed on a stainless steel (INOX-309) plate and placed into an oven at 20 °C for 24 h at atmospheric pressure. After the drying step, sample thickness was measured using a thickness controller (KAEFER trademark BLET—10 mm diameter). Microstructure of the DWCNT hydrogel: dry DWCNT-AG hydrogel nanocomposite was first metallized by sputtering with ca. 2 nm of platinum (Pt JEOL JFC-2300HR) and observed with FEG SEM JEOL JSM 7800F Prime—EDS at 3 kV.

Swelling Measurements

Hydrogel sample was placed in a beaker and was immersed in 10 mL of buffer solution (phosphate citrate buffer Pearse 1980) at 25 °C with 4 different pH, respectively: 4, 5, 6, 7, and phosphate buffer saline at pH 7.4 (PBS without Ca²⁺ and Mg²⁺—Eurobio). Evaluation of swelling was performed to measure the weight gain versus time. The hydrogel sample was quickly removed from the beaker at different time intervals, and carefully blotted free of surface water using classical filter paper, weighted on an analytical balance (accuracy 0.0002 g), and reinserted into the swelling solution. The swelling ratio is defined as the fractional weight increase of the hydrogel due to water absorption. It is calculated from the following equation [Eq. (1)]:

$$w(g \cdot g^{-1}) = \frac{W_t - W_d}{W_d} \quad (1)$$

Here, W_d , W_t represent the weight of dried hydrogel material after drying process at “ t_0 ”, the weight of hydrogel materials after swelling at different pH values at time “ t ”.

The recovery-swelling ratio is defined as the fractional weight increase of the hydrogel due to water absorption in relation to the initial mass. The recovery is easily obtained from the swelling equation [Eq. (2)]:

$$\% \text{ Recovery} = \frac{W_t}{W_i} \times 100 \quad (2)$$

Here, W_i , W_t represent the weight of hydrogel materials before drying and the weight of hydrogel materials after swelling at different pH values at time “ t ”, respectively. Finally, to mimic the penetration of a large molecule, we used FITC-D (average mol. wt. 3,000–5,000 Da) from Sigma–Aldrich. The nanocomposite was incubated for swelling in 1 mM FITC-D in PBS.

Kinetics of Release Measurement

FITC-D molecules release was monitored in terms of kinetics and content (concentration and release %). We used a fluorescence spectrometer (Edinburg FLSP920, Excitation Ne: 490 nm BP: 0.8 nm—Emission Visible photomultiplier: 515 nm–1 nm) with a quartz precision cell containing 3.5 mL of artificial sweat to mimic physiological medium. Furthermore, we used magnetic stirring (400 rpm) at ambient temperature (20–22 °C) to keep the solution homogenous. To maintain the sample and monitor the release, we designed and fabricated a nacelle in polylactic acid by 3D printing (3D Makerbot® Replicator 2). Sample was carefully blotted free of surface water using classical filter paper and placed inside the nacelle. The final concentrations were determined by using a calibration curve from FITC-D (1 mM) solutions of known concentrations.

Electrical Characterization

Electrochemical impedance spectroscopy (EIS) measurements were used to determine the resistivity of the nanocomposite material. The solution resistance was obtained by using the Nyquist representation and reading the Real axis part (Z') value intercept and Imaginary part (Z'') relates to the capacitive part. The real axis (Z') value at the low frequency intercept is the sum of the polarization resistance and the solution resistance. Prior to electrical measurements, the hydrogel nanocomposite was quickly and carefully blotted free of surface water using laboratory filter paper and put between two stainless steel electrodes. The relative resistivity was obtained from impedance measurements using a 4294A Precision Impedance Analyser (Agilent Technologies, Palo Alto, CA) in the range of 1 Hz–1 MHz at room temperature and an applied AC voltage of 100 mV.

Electroporation of Mouse Skin

Fresh dorsal skins were withdraw from mice just after euthanasia and immediately laid out on a homemade Teflon™ Franz cell chamber filled with a PBS solution in the receptor compartment (Figure 9a). The nanocomposite hydrogel electrode was placed on the mouse skin (about 5 min after sacrifice) and covered by a thin copper disk electrode (Figure 9b) connected to the generator (ELECTRO cell B10 HVLV, Betatech, France) (Figure 9c). The inter-electrode distance was set at 1.5 cm from the centre of each nanocomposite cylinder. Then, 10 square-wave pulses lasting 20 ms

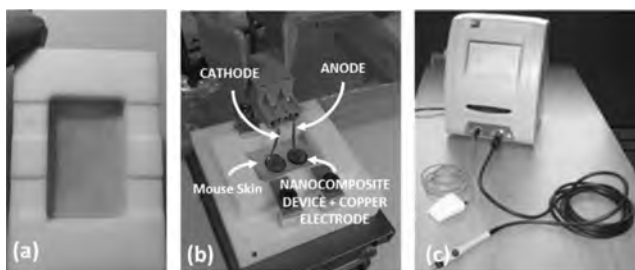


Figure 9. Set-up for electroporation of mouse skin. a) Hairless mouse dorsal skin was set on a homemade Teflon™ Franz cell chamber filled with PBS solution in receptor; (b) DWCNT-AG hydrogel was placed onto on the mouse skin and connected using copper disks. The inter-electrode distance was set at 1 cm from the centre of each nanocomposite cylinder, connected to stainless steel electrodes c) Electroporation generator (ELECTRO cell B10 HVLV).

each, at a pulse repetition rate of 1 Hz, with an amplitude of 300 V, were applied, respectively with CTRL-AG (Control hydrogel agarose) and DWCNT-AG electrodes. Fluorescence optical imaging was performed 30 minutes after pulses directly using a macroscope (Macrofluvo Leica). Selective excitation and emitted fluorescence of FITC was obtained by a filter set GFP1 (Excitation 395–455 nm, emission 480 nm LP Leica Macro Fluvo—Source: Leica EL6000) and detected with a CoolSnap HQ2 CCD camera (Roper Scientific, France). Images were processed for contrast and brightness and analysed with Image J (National Institute of Health, USA).

Acknowledgements

We would like to acknowledge support from the COMUE and Midi-Pyrenees region (grant number 2014-110). Research was conducted in the scope of the EBAM European Associated Laboratory (LEA). We thank the EU funded COST action TD1104. We thank Dr. Serges Mazères for help with fluorescence measurements. We also thank the “Toulouse Réseau Imagerie” and “Anexplo” Core facilities at the IPBS (Genotoul, Toulouse, France). We would like to thank Dr Justin Teissié and Dr Zarel Valdez for their comments and helpful discussions. Finally, we thank the University Paul Sabatier Campus FabLab for assistance with 3D printing.

Conflict of interest

The authors declare no conflict of interest.

Keywords: carbon nanotubes · electrodes · hydrogels · nanocomposites · skin electroporation

[1] J. B. Nielsen, E. Benfeldt, R. Holmgaard, *Curr. Probl. Dermatol.* **2016**, *49*, 103–111.
 [2] M. R. Prausnitz, R. Langer, *Nat. Biotechnol.* **2008**, *26*, 1261–1268.
 [3] G. M. Shingade, Q. Aamer, P. M. Sabale, N. D. Grampurohit, M. V. Gadhav, S. Jadhav, L. D. D. Gaikwad, K. T. Patil, *J. Drug Delivery Ther.* **2012**, *2*, 66–75.
 [4] M. R. Prausnitz, *Crit. Rev. Ther. Drug Carrier Syst.* **1997**, *14*, 455–483.
 [5] S. Mitragotri, *Nat. Rev. Drug Discovery* **2005**, *4*, 255–260.
 [6] M. R. Prausnitz, *Adv. Drug Delivery Rev.* **2004**, *56*, 581–587.
 [7] S. Chabot, J. Teissié, M. Golzio, *Adv Drug Deliv. Rev.* **2015**, *81*, 161–168.

[8] E. Neumann, M. Schaefer-Ridder, Y. Wang, P. H. Hofschneider, *EMBO J.* **1982**, *1*, 841–845.
 [9] L. C. Heller, R. Heller, *Human Gene Therapy* **2006**, *17*, 890–897.
 [10] L. M. Mir, *Methods Mol. Biol.* **2014**, *1121*, 3–23.
 [11] J. L. Young, D. A. Dean, *Adv. Genet.* **2015**, *89*, 49–88.
 [12] M. L. Yarmush, A. Golberg, G. Serša, T. Kotnik, D. Miklavčič, *Annu. Rev. Biomed. Eng.* **2014**, *16*, 295–320.
 [13] M. Cemazar, G. Sersa, *Curr. Opin. Mol. Therapeutics* **2007**, *9*, 554–562.
 [14] N. A. Charoo, Z. Rahman, M. A. Repka, S. N. Murthy, *Curr. Drug Delivery* **2010**, *7*, 125–136.
 [15] N. Dujardin, E. Staes, Y. Kalia, P. Clarys, R. Guy, V. Preat, *J. Controlled Release* **2002**, *79*, 219–227.
 [16] A. Sharma, M. Kara, F. R. Smith, T. R. Krishnan, *J. Pharm. Sci.* **2000**, *89*, 536–544.
 [17] T. E. Zewert, U. F. Pliquet, R. Vanbever, R. Langer, J. C. Weaver, *Bioelectrochem. Bioenerg.* **1999**, *49*, 11–20.
 [18] R. Vanbever, V. Prémat, *Methods Mol. Med.* **2000**, *37*, 457–471.
 [19] T. E. Vaughan, J. C. Weaver, *Methods Mol. Med.* **2000**, *37*, 187–211.
 [20] T. Chen, R. Langer, J. C. Weaver, *J. Invest. Dermatol. Symp. Proc.* **1998**, *3*, 159–165.
 [21] K. Ita, *Pharmaceutics* **2016**, *8*, 9.
 [22] T. García-Sánchez, A. Azan, I. Leray, J. Rosell-Ferrer, R. Bragos, L. M. Mir, *Bioelectrochemistry* **2015**, *105*, 123–135.
 [23] S. Becker, B. Zorec, D. Miklavčič, N. Pavšelj, *Math. Biosci.* **2014**, *257*, 60–68.
 [24] A. R. Denet, R. Vanbever, V. Prémat, *Adv. Drug Delivery Rev.* **2004**, *56*, 659–674.
 [25] A. Paganin-Gioanni, E. Bellard, J. M. Escoffre, M. P. Rols, J. Teissie, M. Golzio, *Proc. Natl. Acad. Sci. USA* **2011**, *108*, 10443–10447.
 [26] L. Daugimont, N. Baron, G. Vandermeulen, N. Pavšelj, D. Miklavci, M. C. Jullien, V. Prémat, *J. Membr. Biol.* **2010**, *236*, 117–125.
 [27] A. Donate, R. Heller, *Bioelectrochemistry* **2013**, *94*, 1–6.
 [28] T. W. Wong, T. Y. Chen, C. C. Huang, J. C. Tsai, S. W. Hui, *Diabetes Technol. Therapeutics* **2011**, *13*, 929–935.
 [29] T. Blagus, B. Markelc, M. Cemazar, T. Kosjek, V. Preat, D. Miklavcic, G. Sersa, *J. Controlled Release* **2013**, *172*, 862–871.
 [30] T. R. Hoare, D. S. Kohane, *Polymer* **2008**, *49*, 1993–2007.
 [31] N. Bhattarai, J. Gunn, M. Zhang, *Adv. Drug Delivery Rev.* **2010**, *62*, 83–99.
 [32] A. S. Hoffman, *Adv. Drug Delivery Rev.* **2012**, *64*, 18–23.
 [33] M. Hamidi, A. Azadi, P. Rafiei, *Adv. Drug Delivery Rev.* **2008**, *60*, 1638–1649.
 [34] G. Cirillo, S. Hampel, U. G. Spizzirri, O. I. Parisi, N. Picci, F. Iemma, *Biomed Res. Internat.* **2014**, 825017.
 [35] M. Karimi, N. Solati, M. Amiri, H. Mirshekari, E. Mohamed, M. Taheri, A. Ghasemi, *Expert Opin. Drug Delivery* **2015**, *12*, 1071–1087.
 [36] E. Flahaut, R. Bacsa, A. Peigney, C. Laurent, *Chem. Commun.* **2003**, 1442–1443.
 [37] A. Bédier, F. Seichepine, E. Flahaut, I. Loubinoux, L. Vaysse, C. Vieu, *Langmuir* **2012**, *28*, 17363–17371.
 [38] C. Strasinger, K. S. Paudel, J. Wu, D. Hammell, R. R. Pinninti, B. J. Hinds, A. Stinchcomb, *J. Pharm. Sci.* **2014**, *103*, 1829–1838.
 [39] A. Servant, V. Leon, D. Jasim, L. Methven, P. Limousin, E. V. Fernandez-Pacheco, K. Kostarelos, *Adv. Healthcare Mater.* **2014**, *3*, 1334–1343.
 [40] A. Servant, L. Methven, R. P. Williams, K. Kostarelos, *Adv. Healthcare Mater.* **2013**, *2*, 806–811.
 [41] S. Barrau, Ph. Demont, A. Peigney, Ch. Laurent, C. Lacabanne, *Macromolecules* **2003**, *36*, 5187–5194.
 [42] S. Mazères, D. Sel, M. Golzio, G. Pucihar, Y. Tamzali, D. Miklavcic, J. Teissié, *J. Controlled Release* **2009**, *134*, 125–123.
 [43] P. C. Lee, C. L. Peng, M. J. Shieh, *J. Controlled Release* **2016**, *225*, 140–151.
 [44] L. Wang, D. Liu, R. Zhou, Z. Wang, A. Cuschieri, *Int. J. Mol. Sci.* **2015**, *16*, 6890–6901.